NeuroImage: Clinical 10 (2016) 283–290

Contents lists available at ScienceDirect

NeuroImage: Clinical

journal homepage: www.elsevier.com/locate/ynicl

Regional brain stiffness changes across the Alzheimer's disease spectrum☆

Matthew C. Murphy[a], David T. Jones[a,b], Clifford R. Jack Jr.[a], Kevin J. Glaser[a], Matthew L. Senjem[a], Armando Manduca[c], Joel P. Felmlee[a], Rickey E. Carter[d], Richard L. Ehman[a], John Huston III[a,*]

[a]Department of Radiology, Mayo Clinic College of Medicine, 200 First Street SW, Rochester, MN 55905, USA
[b]Department of Neurology, Mayo Clinic College of Medicine, 200 First Street SW, Rochester, MN 55905, USA
[c]Department of Physiology and Biomedical Engineering, Mayo Clinic College of Medicine, 200 First Street SW, Rochester, MN 55905, USA
[d]Department of Health Sciences Research, Mayo Clinic College of Medicine, 200 First Street SW, Rochester, MN 55905, USA

ARTICLE INFO

Article history:
Received 5 November 2015
Received in revised form 11 December 2015
Accepted 15 December 2015
Available online 19 December 2015

Keywords:
MR elastography
Brain stiffness
Regional
Alzheimer's disease
Functional connectivity

ABSTRACT

Magnetic resonance elastography (MRE) is an MRI-based technique to noninvasively measure tissue stiffness. Currently well established for clinical use in the liver, MRE is increasingly being investigated to measure brain stiffness as a novel biomarker of a variety of neurological diseases. The purpose of this work was to apply a recently developed MRE pipeline to measure regional brain stiffness changes in human subjects across the Alzheimer's disease (AD) spectrum, and to gain insights into the biological processes underlying those stiffness changes by correlating stiffness with existing biomarkers of AD. The results indicate that stiffness changes occur mostly in the frontal, parietal and temporal lobes, in accordance with the known topography of AD pathology. Furthermore, stiffness in those areas correlates with existing imaging biomarkers of AD including hippocampal volumes and amyloid PET. Additional analysis revealed preliminary but significant evidence that the relationship between brain stiffness and AD severity is nonlinear and non-monotonic. Given that similar relationships have been observed in functional MRI experiments, we used task-free fMRI data to test the hypothesis that brain stiffness was sensitive to structural changes associated with altered functional connectivity. The analysis revealed that brain stiffness is significantly and positively correlated with default mode network connectivity. Therefore, brain stiffness as measured by MRE has potential to provide new and essential insights into the temporal dynamics of AD, as well as the relationship between functional and structural plasticity as it relates to AD pathophysiology.

1. Introduction

Alzheimer's disease (AD) is characterized clinically by the progressive impairment of cognitive function typically beginning with episodic memory, and pathologically by extracellular amyloid plaques and intracellular neurofibrillary tangles (McKhann et al., 1984). The single biggest risk factor is old age and therefore the number of affected individuals in the industrialized world continues to grow as demographics shift toward an older population (Hebert et al., 2003). AD biomarkers are important tools to improve understanding of disease etiology, aid in early diagnosis and provide metrics for the testing of candidate therapies. In fact, biomarkers have already been incorporated into the most recent criteria for the diagnosis of AD (McKhann et al., 2011), as well as mild cognitive impairment (MCI) due to AD (Albert et al., 2011), and pre-clinical AD (Sperling et al., 2011). Most research on AD biomarkers has concentrated on 5 major modalities. These biomarkers measure 2 different processes associated with the AD cascade: 1. Fibrillar amyloid beta deposition (measured by amyloid positron emission tomography [PET] imaging or cerebrospinal fluid [CSF] assay); and 2. Tau-mediated neurodegeneration (measured by CSF assay, fluorodeoxyglucose 18F [FDG] PET, and structural MRI).

Based on these modalities, Jack et al. proposed a model of dynamic biomarkers across the AD spectrum, which hypothesized that the biomarkers progress monotonically from normal to abnormal in a characteristic temporal sequence (Jack et al., 2010, 2013). This model provides a theoretical framework for how to use multimodal biomarker data to measure an individual's position along the spectrum of AD severity, and work is ongoing to validate the model. However, these 5 biomarkers certainly do not measure all biological processes associated with Alzheimer's disease, and novel biomarkers that measure additional processes would improve the model. Notably, the model does not currently include direct measures of functional and structural connectivity.

Previously, we reported that global brain stiffness as measured by magnetic resonance elastography (MRE) was decreased in subjects with AD compared to age-matched control subjects both with and without a significant brain amyloid load (Murphy et al., 2011). MRE is an

☆ Classification: biological sciences

* Corresponding author at: 200 First Street Southwest, Rochester, MN 55905, USA.
E-mail address: jhuston@mayo.edu (J. Huston).

http://dx.doi.org/10.1016/j.nicl.2015.12.007

MRI-based technique to noninvasively measure tissue stiffness (Muthupillai et al., 1995). It is a three step process beginning with the introduction of shear waves into the tissue of interest via an external vibration source. The resulting shear waves are imaged with a phase-contrast MRI pulse sequence by applying motion-encoding gradients that are synchronized to the external vibrations. Finally, the shear wave images are mathematically inverted to calculate a stiffness map, which is also called an elastogram. MRE is already used clinically to measure liver disease severity from the early stages of fibrosis through cirrhosis (Yin et al., 2007). More recently, several groups have begun to apply MRE to the brain to measure the effects of age and sex on brain structure (Arani et al., 2015; Sack et al., 2009), or to investigate the potential of brain stiffness as a novel biomarker of a number of neurological diseases including multiple sclerosis (Streitberger et al., 2012; Wuerfel et al., 2010), normal pressure hydrocephalus (Freimann et al., 2012; Streitberger et al., 2011), intracranial tumors (Murphy et al., 2012b; Xu et al., 2007), and amyotrophic lateral sclerosis (Romano et al., 2014).

The purpose of this work was to measure the relationship between brain stiffness and severity of AD pathophysiology along the entire disease spectrum, and to gain further insight into the biological processes underlying changes in brain stiffness due to AD. To date only measures of global brain stiffness in AD have been studied systematically and elastography thus remains a largely unexplored and potentially unique window into the biological expression of the disease. These aims, respectively, were accomplished by applying recently developed MRE techniques to measure regional brain stiffness in subjects spanning the AD spectrum (i.e., cognitively normal → mild cognitive impairment → AD dementia), and then investigating the relationships between brain stiffness and existing biomarkers.

2. Materials and methods

2.1. Subject recruitment

This study was approved by our institutional review board. After obtaining informed written consent, we scanned 48 subjects in 4 age- and gender-matched groups including 16 amyloid-negative cognitively normal controls (CN−, 8 male, 8 female), 16 amyloid-positive cognitively normal controls (CN+, 8 male, 8 female), 8 amyloid-positive subjects with mild cognitive impairment (MCI, 4 male, 4 female), and 8 amyloid-positive subjects with probable Alzheimer's disease (AD, 6 male, 2 female). These subjects were recruited from the Mayo Clinic Study of Aging (MCSA) and the Alzheimer's Disease Patient Registry. Criteria for the diagnosis of cognitively normal control subjects included: 1. no active neurologic or psychiatric disorders; 2. absence of any ongoing medical problems or their treatments that may interfere with cognitive function; 3. a normal neurological exam; 4. no psychoactive medications; and 5. were independently functioning community dwellers. The diagnosis of probable Alzheimer's disease was made according to the Diagnostic and Statistical Manual for Mental Disorders, III Edition—Revised (DSM-III-R) Criteria for dementia, and National Institute of Neurological and Communicative Disorders and Stroke/Alzheimer's Disease and Related Disorders Association Criteria (NINCDS/ADRDA) for AD. To ensure the MCI and AD groups had AD pathology, the subjects also were required to have tested positive for brain amyloid load (i.e., PIB SUVR > 1.5).

2.2. PET scans

Quantitative image analysis for PIB PET was done using an in-house, fully automated image processing pipeline as previously described (Jack et al., 2008). Statistics on image voxel values were extracted from automatically labeled cortical ROIs using an in-house modified version of the AAL atlas (Tzourio-Mazoyer et al., 2002). A cortical amyloid PET standardized uptake value ratio (SUVR) was formed by combining the prefrontal, orbitofrontal, parietal, temporal, anterior cingulate, and posterior cingulate/precuneus ROI values normalized by the cerebellar gray matter ROI of the atlas. The cut-off of 1.5 PIB SUVR for amyloid positivity was previously determined as the optimal threshold for separating high versus low amyloid PET values measured in sample including CN, MCI and AD subjects (Jack et al., 2008).

2.3. MRE acquisition

MRE images were collected with a modified single-shot spin-echo EPI pulse sequence on a 3 T MR imager (SIGNA Excite, GE Healthcare, Waukesha, WI). Shear waves of 60 Hz were introduced into the brain as previously described (Murphy et al., 2011). This system is comprised of an active pneumatic driver (located outside the scanner room), which vibrates a soft, pillow-like passive driver placed under the subject's head. The resulting displacement field was imaged with the following parameters: TR/TE = 3600/62 ms; FOV = 24 cm; BW = ±250 kHz; 72 × 72 imaging matrix reconstructed to 80 × 80; frequency encoding in the right-left direction; 3× parallel imaging acceleration; 48 contiguous 3 mm thick axial slices; one 4 G/cm, 18.2 ms, zeroth- and first-order moment nulled motion-encoding gradient on each side of the refocusing RF pulse synchronized to the motion; motion encoding in the positive and negative x, y and z directions; and 8 phase offsets sampled over one period of the 60 Hz motion. The resulting images have 3 mm isotropic resolution and were acquired in just less than 7 min. Two additional phase offsets with the motion turned off were acquired for subsequent signal-to-noise ratio (SNR) calculations.

2.4. Image processing

The MRE pipeline for measuring regional brain stiffness has been previously detailed, along with an evaluation of its test–retest reliability in young volunteers (Murphy et al., 2013). First, complex phase-difference images in each of the x, y and z motion-encoding directions were calculated by taking the product of the complex-valued image with positive motion encoding and the complex conjugate of the image with negative motion encoding. To reduce slice-to-slice phase discontinuities, constant and slowly varying phase ramps in the acquisition plane were removed by first applying a 2D low pass filter (3 × 3 rectangular window function in k-space) to the complex phase difference images (Murphy et al., 2012a). Wave images were then calculated as the phase-difference between the original complex phase difference images and the low pass-filtered phase difference images.

To create the regions of interest (ROIs) and a brain mask we used a separately acquired T1-weighted IR-SPGR image that was collected with the following parameters: sagittal orientation; frequency encoding in the superior–inferior direction; TR/TE = 6.3/2.8 ms; flip angle = 11°; TI = 400 ms; FOV = 27 cm; 256 × 256 acquisition matrix; BW = ±31.25 kHz; 1.75× parallel imaging acceleration in the anterior–posterior direction; and 200 1.2-mm slice locations. A lobar atlas in a standard template space was warped to the subject's T1 image using a unified segmentation algorithm implemented in SPM5 (Ashburner and Friston, 2005). This algorithm also segmented the T1-weighted image to calculate maps of gray matter (GM), white matter (WM), and cerebrospinal fluid (CSF) content in each voxel. The T1-weighted image along with the lobar atlas and the segmentation images were then registered (6 degree of freedom rigid body transformation) and resliced to the T2-weighted magnitude image from the MRE data in order to calculate the regional assignment and the GM, WM and CSF content in each voxel in MRE space. A brain mask was generated by including any voxel in which GM plus WM content was greater than CSF content. The T1-weighted image was also used to calculate hippocampal volumes using FreeSurfer for later use as an established measure of disease severity (Fischl et al., 2002). One scan failed this process, and so

analyses that included hippocampal volumes were performed on the remaining 47 subjects.

Stiffness was calculated in 9 large, bilateral ROIs to maintain high test–retest reliability: global (whole brain excluding cerebellum), frontal lobes, occipital lobes, parietal lobes, temporal lobes, deep GM/WM (insula, deep gray nuclei and white matter tracts), cerebellum, sensory/motor strip (pre- and post-central gyri), and a composite region labeled FPT (frontal, parietal and temporal lobes excluding the pre- and post-central gyri). For each region, the wave images were first masked with the ROI, which was the intersection of the atlas region and the brain mask. Using recently developed adaptive methods, the curl of the wave images was calculated to eliminate the effects of longitudinal waves, and the curl images were smoothed with a filter of the form $(1\text{-}x^2)^2(1\text{-}y^2)^2(1\text{-}z^2)^2$, where x, y, and z are linearly spaced from − 1 to 1 over 5 × 5 × 5 window (Murphy et al., 2013; Romano et al., 2000). Since the evaluation of this function is equal to zero along all edges, the effective filter kernel has a size of 3 × 3 × 3. Finally a stiffness map was calculated by direct inversion of the Helmholtz equation that models shear wave motion in a homogeneous, linear, viscoelastic material (Manduca et al., 2001). Stiffness was calculated as the median from the ROI after excluding one voxel from the surface of the region mask to eliminate edge-related bias. Finally, the median stiffness was corrected for SNR using a previously described iterative approach. This approach has been shown in reproducibility studies to provide coefficient of variation of less than 1% for global brain stiffness and less than 2% for the lobes of the brain and the cerebellum (Murphy et al., 2013). For display purpose only, the stiffness maps were smoothed with a 3 × 3 × 3 median filter.

2.5. Task-free functional MRI acquisition, preprocessing, and analysis

Task-free fMRI data were acquired using a General Electric 3 T Signa HDx scanner, 8 channel head coil, gradient EPI, TR = 3000 ms, TE = 30 ms, 90° flip angle, 21 cm field of view, 64 × 64 in-plane matrix, slice thickness 3.3 mm without gap, and 113 volumes were obtained. Subjects were instructed to keep their eyes open during scanning. All TF-fMRI data sets with greater than 3 mm of translational movement, 3° of rotational movement, or that failed visual inspection for obvious artifacts were excluded from analysis. Preprocessing was performed utilizing a combination of the Statistical Parametric Mapping (SPM5) software (http://www.fil.ion.ucl.ac.uk/spm/software/spm5/) (Wellcome Department of Cognitive Neurology, University College London, UK), the Resting-State fMRI Data Analysis Toolkit (REST) v1.5 (http://www.restfmri.net) (Song et al., 2011), Data Processing Assistant for Resting-State fMRI (DPARSF) v2.0 (http://www.restfmri.net) (Chao-Gan and Yu-Feng, 2010), group ICA of fMRI toolbox (GIFT) software v2.0c (http://icatb.sourceforge.net) (Calhoun et al., 2001b), and in-house developed software implemented in MATLAB v7.11 (Mathworks Inc., Natick, MA, USA).

Preprocessing steps included discarding the first 3 volumes to obtain steady state magnetization, slice time correction, realignment, normalization to SPM5 EPI template, smoothing with 4 mm full-width half maximum Gaussian kernel, linear detrending to correct for signal drift, and 0.01–0.08 Hz bandpass filtering to reduce non-neuronal contributions to blood-oxygenation-level-dependent (BOLD) signal fluctuations (Fox et al., 2009; Weissenbacher et al., 2009). In addition, linear regression correction for spurious variables included rigid body transformation motion effects and the first seven principle components of the voxel-wise time courses within white matter and cerebral spinal fluid regions of interest derived from their respective template space priors (Behzadi et al., 2007).

The anterior default mode network (aDMN) was back-reconstructed for each subject using the spatial-temporal dual regression method implemented in the GIFT software package (Calhoun et al., 2001a). The aggregate group independent component analysis (GICA) aDMN template from the high-dimensional ICA MCSA functional atlas was used for the back-reconstruction (available at http://mayoresearch.mayo.edu/mayo/research/jack_lab/supplement.cfm) (Jones et al., 2012). Back-reconstructed maps were scaled to z-scores for each subject. For our measure of anterior-to-posterior (A–P) DMN connectivity we used the midline posterior DMN (pDMN) ROIs from the MCSA functional atlas and extracted the median z-score within this ROI from each subject's back-reconstructed aDMN maps.

2.6. Statistical analysis

All variables were corrected for age by first fitting the values versus age by linear regression, calculating the residuals, and finally adding a constant term (the value of the linear regression evaluated at age 80). Group-wise differences in the median stiffness between the CN and AD groups were tested by region using the Wilcoxon rank sum test (Devore, 2012). After establishing a summary ROI, the Kruskal–Wallis test was used to determine if at least one of the 4 groups had a median stiffness different from the others (Devore, 2012). Subsequent *post hoc* comparisons were again made with the Wilcoxon rank sum test. Correlations were tested by Spearman rank correlation. To estimate the functional form of these relationships, we selected one of four models (linear or restricted cubic splines with 3, 4 or 5 knots) that minimized Akaike's information criterion (Akaike, 1974). These models were further evaluated with an F test and the corresponding p values are reported in the Results section (Devore, 2012). For display, regression model figures include the mean fit (solid line) and 95% confidence intervals (dotted lines) calculated using 10,000 bootstrap samples.

3. Results

3.1. Changes in brain stiffness follow the known topography of AD

We measured regional brain stiffness in four age- and gender-matched groups: 16 amyloid PET-negative cognitively normal controls (CN−), 16 amyloid PET-positive cognitively normal controls (CN+), 8 amyloid PET-positive subjects with mild cognitive impairment (MCI) due to AD, and 8 amyloid PET-positive subjects with AD dementia. Example images from a subject in the CN− group are shown in Fig. 1.

Summary results by region are shown for all 32 CN subjects versus the 8 subjects with AD dementia in Fig. 2 (mean ± standard deviation after age correction) and listed in Table 1. This study reproduces the previous finding that global brain stiffness is decreased in subjects with AD dementia compared to control subjects (Murphy et al., 2011). Furthermore, group-wise differences in stiffness were observed within the lobes of the brain that contain primarily hetero modal association cortices ($p < 0.01$ in the frontal and temporal lobes, $p = 0.056$ in the parietal lobes), but not throughout the rest of the brain ($p > 0.1$, occipital lobes, sensory/motor strip, deep gray and white matter, and the cerebellum). Based on these results, we generated an optimized meta-region of interest (ROI) for CN and AD group-wise discrimination that included the frontal, parietal and temporal lobes but excluded the pre- and post-central gyri, which is labeled FPT in Fig. 2. FPT stiffness for each of the four groups is summarized in Fig. 3. A Kruskal–Wallis test indicates that the groups are different from one another ($p = 0.020$), and subsequent pair-wise comparisons indicate that subjects with AD have decreased stiffness compared to both the CN− ($p = 0.0013$) and CN+ ($p = 0.011$) groups. This ROI outperforms all others for discriminating the two groups. Receiver operating characteristic curve (ROC) analysis indicates an area under the curve of 0.871 and accuracy of 85.0%.

3.2. Stiffness decreases with increasing disease severity as measured by standard AD imaging biomarkers across all subjects

To gain insight into how brain stiffness changes may progress along the spectrum of AD, we evaluated brain stiffness against two other well accepted continuous imaging measures of disease severity. As

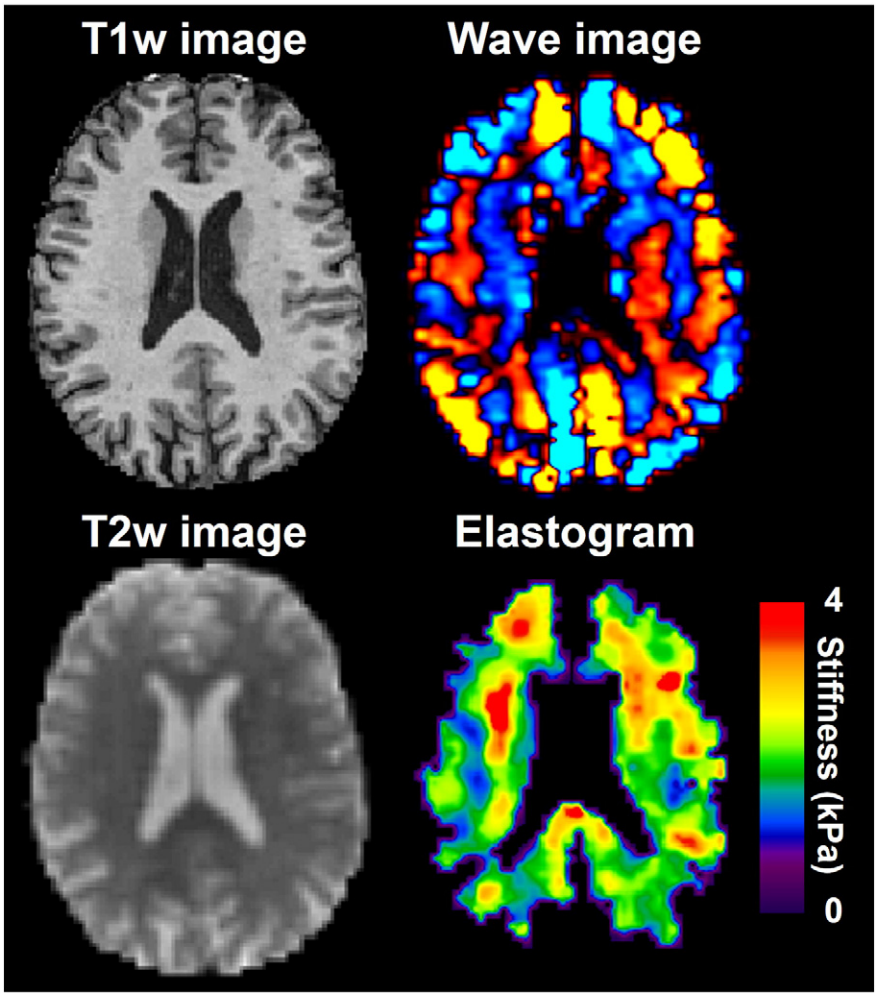

Fig. 1. Example MRE images from a cognitively normal control. The T1-weighted (T1w) image is shown in the top-left panel, and the T2-weighted (T2w) MRE magnitude image is shown in the bottom-left. A curl wave image is shown in the top-right panel, along with the resulting elastogram in the bottom-right panel.

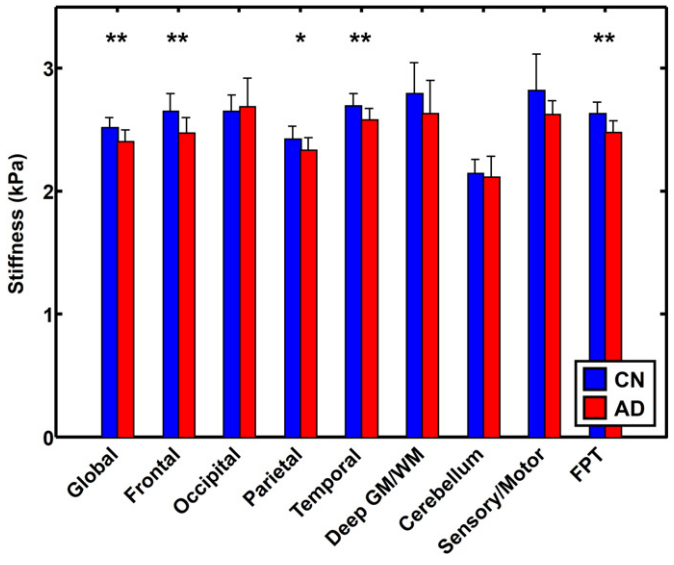

Fig. 2. Summary of stiffness in CN subjects versus subjects with AD. Stiffness was measured in 9 regions of interest. The bars represent the mean stiffness of the subjects in each group (32 CN versus 8 AD), while the error bars represent the standard deviation. Significant differences were observed in the global, frontal lobe, temporal lobe, and FPT regions (**$p < 0.01$), and trend level significance was observed in the parietal lobe region (*$p = 0.056$).

hypothesized, changes in brain stiffness correlated continuously with these established measures of AD severity. More specifically, brain stiffness positively correlated with hippocampal volume ($R = 0.50$, $p = 4.6e\text{-}4$, Spearman rank correlation), while stiffness was negatively correlated with PIB SUVR ($R = -0.32$, $p = 0.027$).

3.3. Preliminary within-group evidence suggests that brain stiffness changes non-monotonically across the AD spectrum

Among all MCI subjects, around 60% are amyloid positive (Jack et al., 2008), thus only 60% would be considered etiologically to have "MCI due to AD" using current diagnostic criteria from the National Institute

Table 1
Summary of regional stiffness in cognitively normal and AD groups.

ROI	Stiffness (kPa, mean ± standard deviation)		Cohen's d
	CN	AD	
Global	2.51 ± 0.09	2.40 ± 0.09	1.26
Frontal	2.65 ± 0.15	2.47 ± 0.12	1.23
Occipital	2.65 ± 0.13	2.68 ± 0.24	−0.23
Parietal	2.42 ± 0.10	2.33 ± 0.10	0.88
Temporal	2.69 ± 0.11	2.58 ± 0.09	1.04
Deep GM/WM	2.79 ± 0.25	2.63 ± 0.27	0.64
Cerebellum	2.15 ± 0.11	2.11 ± 0.17	0.26
Sensory/Motor	2.82 ± 0.29	2.62 ± 0.11	0.73
FPT	2.63 ± 0.10	2.48 ± 0.09	1.51

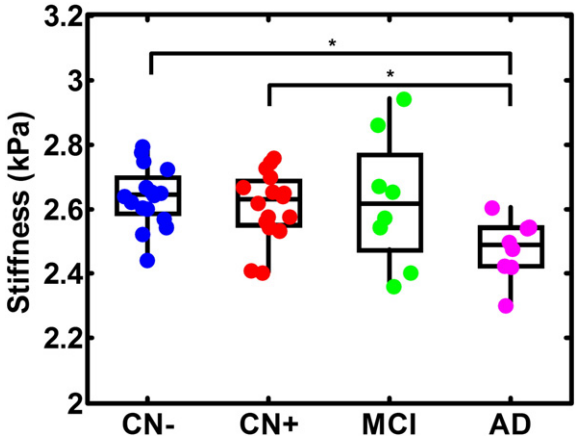

Fig. 3. Summary of FPT stiffness by group. Each marker represents one subject, the horizontal lines represent the group median, the boxes represent the interquartile range, and the whiskers represent the range. A Kruskal–Wallis test indicated that at least one group was different from the others ($p = 0.02$), and *post hoc* Wilcoxon rank sum tests indicated the AD group was significantly softer than both the CN groups (*$p < 0.05$).

of Aging and Alzheimer's Association (NIA-AA) (Albert et al., 2011). For this reason we included only amyloid PET positive subjects in our MCI group and all of our MCI subjects therefore meet NIA-AA criteria for MCI due to AD. Thus our elastography findings in MCI reflect an etiologically pure group that lies between CN+ and AD dementia on the disease severity spectrum. Our 4 groups of subjects then would array themselves from least to most severe along the AD disease spectrum as follows: CN− (uninvolved), CN+ (earliest involvement), MCI (intermediate involvement), and AD dementia (most involvement).

Unexpectedly, stiffness within the MCI group was not intermediate between the control subjects and those with AD (Fig. 3). Stiffness within the MCI group was highly variable, ranging from the stiffest within the entire study to well within the range of subjects with AD. However, stiffness within this group was highly predicted by both amyloid load as measured by PIB SUVR ($R = -0.86$, $p = 0.011$, Spearman rank correlation), as well as by hippocampal volume ($R = 0.88$, $p = 0.0072$). The signs of these correlations suggest that stiffness spikes at the onset of MCI (i.e., subjects with MCI but relatively low disease severity as assessed by biomarkers) before falling to the levels observed in AD, and example stiffness maps demonstrating this relationship between stiffness and AD severity are shown in Fig. 4.

To further investigate this relationship, we again separated the subjects into four groups (CN−, CN+, MCI and AD) and performed an ANCOVA on stiffness versus PIB SUVR. This test indicated that the stiffness versus PIB relationship was different between groups ($p < 0.001$). Subsequently we tested each group for significant stiffness versus PIB relationships and found significant correlations in each of the CN− and MCI groups and trend level significance in the CN+ group (Fig. 5). Furthermore, the sign of those correlations alternates as the groups progress along the AD spectrum. Stiffness decreases with increasing amyloid load in the CN− group ($R = -0.72$, $p = 0.0024$, Spearman rank correlation), then increases with increasing amyloid in the CN+ group ($R = 0.47$, $p = 0.066$), and then again decreases with increasing amyloid load in the MCI group ($R = -0.86$, $p = 0.011$). No significant relationship was observed between stiffness and amyloid load in the AD group ($R = -0.26$, $p = 0.54$).

Non-monotonic relationships were also observed using restricted cubic splines to fit the relationship between stiffness and existing biomarkers. The fits with the optimal number of knots as determined by Akaike's information criterion (AIC) are shown in Fig. 6. Brain stiffness versus amyloid load showed a significant non-monotonic relationship (middle panel, $R^2 = 0.22$, F-test $p = 0.011$), just as it does versus hippocampal volumes (top panel, $R^2 = 0.36$, F-test $p = 0.00065$).

3.4. Brain stiffness is associated with functional connectivity

Similar non-monotonic relationships have been reported in functional MRI experiments of subjects with MCI and AD, both with a memory task (Putcha et al., 2011), and in changes to intrinsic connectivity networks (Bai et al., 2011). Given the above evidence of non-monotonic changes in brain stiffness across the AD spectrum, we hypothesized that brain stiffness was sensitive to structural alterations that were associated with changes in functional connectivity. To test this hypothesis, we used task-free functional MRI (TF-fMRI) scans that were collected as part of the previously mentioned study. Since changes in brain stiffness were most prominent in the frontal lobes, we focused on the anterior default mode network (aDMN). Maps of aDMN connectivity were generated for each subject by performing a back reconstruction technique utilizing templates from a previously conducted large group independent component analysis (Calhoun et al., 2001b). From these aDMN maps, we extracted the mean connectivity with a region of interest (ROI) within the posterior DMN (pDMN) as a measure of anterior-to-posterior (A–P) DMN connectivity, given the mounting evidence of the importance of disrupted A–P DMN connectivity across the AD spectrum (Jones et al., 2011, 2012; Liu et al., 2013). Brain stiffness

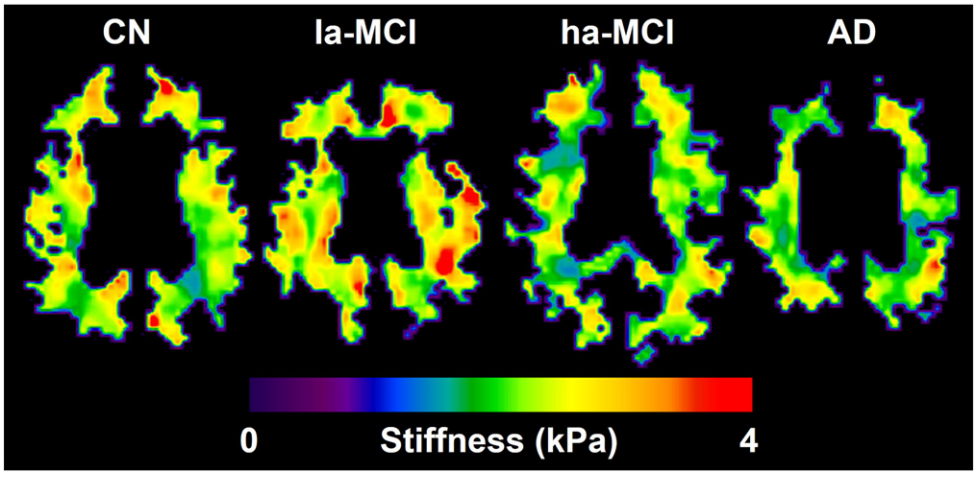

Fig. 4. Example elastograms across the AD spectrum. Relative to a CN control subject, stiffness is elevated in low (but still positive)-amyloid subjects with MCI (la-MCI) before falling in high-amyloid subjects with MCI (ha-MCI) to levels that are common within the AD group.

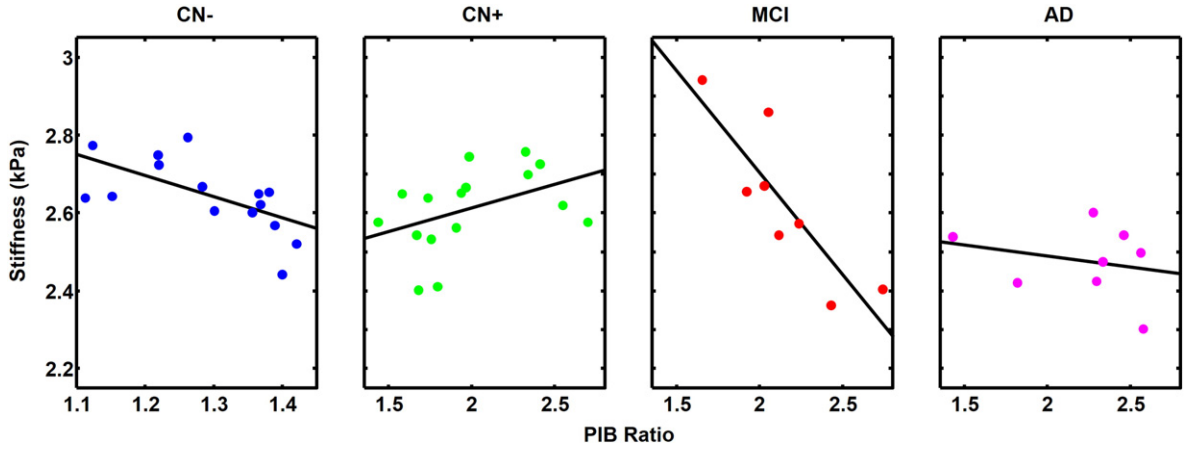

Fig. 5. Stiffness versus PIB SUVR by group. An ANCOVA showed that the relationship between stiffness and PIB SUVR is significantly different between groups ($p < 0.001$). The alternating sign of the correlations is preliminary evidence that the relationship between brain stiffness and AD severity is nonlinear and non-monotonic.

was significantly correlated with this measure of A–P DMN connectivity ($R = 0.31$, Spearman correlation $p = 0.035$). There was no evidence of a nonlinear or non-monotonic relationship between stiffness and A–P DMN connectivity as a linear model minimized AIC (Fig. 6, bottom panel).

4. Discussion

This work represents the first study comparing regional brain stiffness to other standard biomarkers across the spectrum of AD. These results reproduce our previous finding that global brain stiffness is decreased due to AD (Murphy et al., 2011), and then expand the scope of the investigation to earlier stages of the AD pathophysiological cascade. Furthermore, this study utilizes a newly developed regional MRE pipeline, which possesses strong test–retest reliability with a typical coefficient of variation of <1% for measuring global brain stiffness and <2% for measuring regional stiffness. Moreover, this pipeline is resistant to noise- and edge-related biases, allowing this technique to accurately measure stiffness independent of effects related to atrophy (Murphy et al., 2013). These regional results indicate that brain stiffness is both sensitive to AD pathophysiology by detecting significant group-wise differences in regions known to be affected by the disease, and also specific since regions that are relatively unaffected by the disease show no group-wise differences (Arnold et al., 1991; Braak and Braak, 1991).

In general, our results indicate that brain stiffness decreases with increasing AD severity by using existing imaging biomarkers as a continuous variable to define each individual's position along the AD spectrum. The more unexpected result is the preliminary, but significant, evidence of a non-monotonic relationship between brain stiffness and AD pathophysiological severity when severity is characterized by both clinical group and AD biomarker values. As this study was based on a relatively small number of subjects and cross-sectional data, further investigations will be needed to corroborate that at least some aspects of the AD pathophysiologic cascade follow not only nonlinear, but non-monotonic time courses.

The existence of such relationships would have a number of impacts on the field of biomarkers of AD. For example, group-wise discrimination alone is likely a suboptimal method for evaluating a non-monotonic biomarker as such biomarkers may or may not exhibit significant group-wise differences. Consider brain stiffness in the CN−, CN+, and MCI groups presented in this work. While the median stiffness values within those groups were not significantly different from one another, the relationship between stiffness and amyloid load was significantly different between groups. This type of relationship may also explain at least in part why some biomarkers are more accurate for group-wise discrimination than others. The effect size of CN and AD group-wise differences may be reduced due to a non-monotonic time course when compared to a biomarker with a monotonic time course. Furthermore, non-monotonic time courses and the distribution of their frequency spectra must be well understood in order to properly design longitudinal studies. If the time between follow-up scans is not sufficiently short, the functional form of the biomarker's time course will be altered. While these alterations may be negligible when the biomarker's time courses is monotonic, when the time course is non-monotonic, the resulting shape of the discretely sampled time course can be highly impacted by the sampling rate.

Based on this non-monotonic time course, we hypothesized that brain stiffness was associated with alterations in functional connectivity changes due to AD. We then used TF-fMRI data to show that FPT stiffness was in fact correlated with default mode network connectivity. This association could be cause and effect, or both TF-fMRI and MRE changes could both be due to a common upstream pathological process. The link between functional connectivity and brain stiffness will be the subject of further investigation, but potential processes that could provide this link include white matter and/or cerebrovascular plasticity. Both of these structural changes have been demonstrated in mice when exposed to an enriched environment (Markham and Greenough, 2004). More recent evidence demonstrates that increased neuronal activity promotes oligodendrocyte precursor cell proliferation and myelin thickening in mice (Gibson et al., 2014). Such changes in myelination could be expected to alter both functional connectivity, by increasing conduction speed and in turn modifying the phase of oscillations between two distant nodes, and structural measures of white matter, which may be detectable by either brain stiffness or white matter anisotropy. These two structural measurements have previously been shown to be strongly correlated (Johnson et al., 2013). Given this association, MRE can be used in conjunction with TF-fMRI to study how functional connectivity changes with respect to AD pathophysiology, as well as the relationship between those functional changes and structural plasticity. One advantage brain stiffness may have over metrics based on TF-fMRI is high test-retest reliability, as mentioned above. While TF-MRI connectivity measures are reproducible at the group level, they are less reliable at the individual level due in large part to the non-stationary nature of these networks (Jones et al., 2012). Ultimately we hypothesize that these two types of experiments provide complimentary information where a TF-fMRI experiment provides insight into brain connectivity on the order of seconds to minutes, while brain stiffness reflects, at least in part, the average functional connectivity over a window of weeks or months (assuming time is required for functional changes to be manifested in brain structure).

In summary, we report that brain stiffness is decreased in subjects with AD dementia compared to amyloid positive and negative CN subjects. These changes in brain stiffness are also shown to follow the known topography of the disease. In addition to demonstrating group-

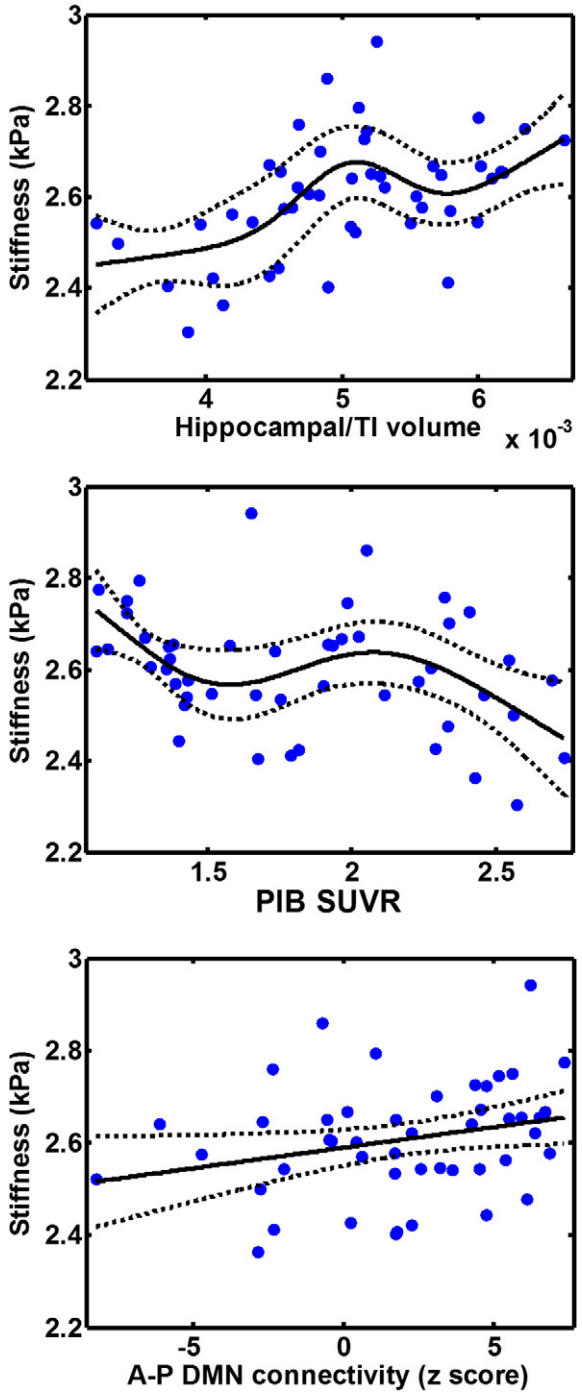

Fig. 6. Restricted cubic spline regression models of stiffness versus standard biomarkers. Top panel: The relationship between stiffness and hippocampal volumes was best fit using 5 knots and was significantly nonlinear ($R^2 = 0.36$, $p = 0.00065$). Middle panel: Stiffness versus PIB SUVR was best fit using 4 knots and was significantly nonlinear ($R^2 = 0.22$, $p = 0.011$). Bottom panel: Stiffness versus A-P DMN connectivity was best fit by linear regression ($R^2 = 0.27$, $p = 0.067$). Lines represent the mean fit (solid line) and 95% confidence intervals (dotted lines) calculated over 10,000 bootstrap samples.

wise differences, brain stiffness is also significantly correlated with existing biomarkers indicating that in general stiffness decreases with increasing AD severity. Furthermore, in this work we show evidence that the relationship between brain stiffness and AD severity is non-linear and non-monotonic. If such a relationship is validated, it will have an important impact on the design of longitudinal studies. Due to this non-monotonic relationship, we used TF-fMRI data to test the hypothesis that brain stiffness was associated with changes in functional connectivity. Our analysis shows that brain stiffness is positively correlated with default mode connectivity, which may reflect structural alterations that are related to functional plasticity that occurs throughout the AD cascade. Therefore, while the application of MRE to AD is in its infancy and requires further investigation, brain stiffness demonstrates potential for characterizing alterations in brain structure with respect to the AD spectrum that existing biomarkers have yet to fully capture.

Acknowledgments

This work was supported by NIH R01 grants EB001981 and AG11378.
Commercial interest
Matthew C. Murphy, Kevin J. Glaser, Armando Manduca, Joel P. Femlee, Richard L. Ehman, John Huston, III and Mayo Clinic have intellectual property rights and a potential financial interest in the technology used in this study.

References

Akaike, H., 1974. A new look at the statistical model identification. IEEE Trans. Autom. Control 19, 716–723.
Albert, M.S., DeKosky, S.T., Dickson, D., Dubois, B., Feldman, H.H., Fox, N.C., Gamst, A., Holtzman, D.M., Jagust, W.J., Petersen, R.C., Snyder, P.J., Carrillo, M.C., Thies, B., Phelps, C.H., 2011. The diagnosis of mild cognitive impairment due to Alzheimer's disease: recommendations from the National Institute on Aging-Alzheimer's Association workgroups on diagnostic guidelines for Alzheimer's disease. Alzheimers Dement. 7, 270–279.
Arani, A., Murphy, M.C., Glaser, K.J., Manduca, A., Lake, D.S., Kruse, S.A., Jack Jr., C.R., Ehman, R.L., Huston III, J., 2015. Measuring the effects of aging and sex on regional brain stiffness with MR elastography in healthy older adults. NeuroImage 111, 59–64.
Arnold, S.E., Hyman, B.T., Flory, J., Damasio, A.R., Van Hoesen, G.W., 1991. The topographical and neuroanatomical distribution of neurofibrillary tangles and neuritic plaques in the cerebral cortex of patients with Alzheimer's disease. Cereb. Cortex 1, 103–116.
Ashburner, J., Friston, K.J., 2005. Unified segmentation. NeuroImage 26, 839–851.
Bai, F., Watson, D.R., Shi, Y., Wang, Y., Yue, C., YuhuanTeng, Wu.D., Yuan, Y., Zhang, Z., 2011. Specifically progressive deficits of brain functional marker in amnestic type mild cognitive impairment. PLoS One 6, e24271.
Behzadi, Y., Restom, K., Liau, J., Liu, T.T., 2007. A component based noise correction method (CompCor) for BOLD and perfusion based fMRI. NeuroImage 37, 90–101.
Braak, H., Braak, E., 1991. Neuropathological stageing of Alzheimer-related changes. Acta Neuropathol. 82, 239–259.
Calhoun, V.D., Adali, T., Pearlson, G.D., Pekar, J.J., 2001a. A method for making group inferences from functional MRI data using independent component analysis. Hum. Brain Mapp. 14, 140–151.
Calhoun, V.D., Adali, T., Pearlson, G.D., Pekar, J.J., 2001b. A method for making group inferences from functional MRI data using independent component analysis. Hum. Brain Mapp. 14, 140–151.
Chao-Gan, Y., Yu-Feng, Z., 2010. DPARSF: A MATLAB Toolbox for "Pipeline" Data Analysis of Resting-State fMRI. Front. Syst. Neurosci. 4, 13.
Devore, J.L., 2012. Probability and Statistics for Engineering and the Sciences. Eighth edition. Brooks/Cole, Boston.
Fischl, B., Salat, D.H., Busa, E., Albert, M., Dieterich, M., Haselgrove, C., van der Kouwe, A., Killiany, R., Kennedy, D., Klaveness, S., Montillo, A., Makris, N., Rosen, B., Dale, A.M., 2002. Whole brain segmentation: automated labeling of neuroanatomical structures in the human brain. Neuron 33, 341–355.
Fox, M.D., Zhang, D., Snyder, A.Z., Raichle, M.E., 2009. The global signal and observed anticorrelated resting state brain networks. J. Neurophysiol. 101, 3270–3283.
Freimann, F.B., Streitberger, K.J., Klatt, D., Lin, K., McLaughlin, J., Braun, J., Sprung, C., Sack, I., 2012. Alteration of brain viscoelasticity after shunt treatment in normal pressure hydrocephalus. Neuroradiology 54, 189–196.
Gibson, E.M., Purger, D., Mount, C.W., Goldstein, A.K., Lin, G.L., Wood, L.S., Inema, I., Miller, S.E., Bieri, G., Zuchero, J.B., Barres, B.A., Woo, P.J., Vogel, H., Monje, M., 2014. Neuronal activity promotes oligodendrogenesis and adaptive myelination in the mammalian brain. Science 344, 1252304.
Hebert, L.E., Scherr, P.A., Bienias, J.L., Bennett, D.A., Evans, D.A., 2003. Alzheimer disease in the US population. Arch. Neurol. 60, 1119–1122.
Jack Jr., C.R., Lowe, V.J., Senjem, M.L., Weigand, S.D., Kemp, B.J., Shiung, M.M., Knopman, D.S., Boeve, B.F., Klunk, W.E., Mathis, C.A., Petersen, R.C., 2008. ^{11}C PiB and structural MRI provide complementary information in imaging of Alzheimer's disease and amnestic mild cognitive impairment. Brain 131, 665–680.
Jack Jr., C.R., Knopman, D.S., Jagust, W.J., Shaw, L.M., Aisen, P.S., Weiner, M.W., Petersen, R.C., Trojanowski, J.Q., 2010. Hypothetical model of dynamic biomarkers of the Alzheimer's pathological cascade. Lancet Neurol. 9, 119–128.
Jack Jr., C.R., Knopman, D.S., Jagust, W.J., Petersen, R.C., Weiner, M.W., Aisen, P.S., Shaw, L.M., Vemuri, P., Wiste, H.J., Weigand, S.D., Lesnick, T.G., Pankratz, V.S., Donohue, M.C., Trojanowski, J.Q., 2013. Tracking pathophysiological processes in Alzheimer's disease: an updated hypothetical model of dynamic biomarkers. Lancet Neurol. 12, 207–216.

Johnson, C.L., McGarry, M.D., Gharibans, A.A., Weaver, J.B., Paulsen, K.D., Wang, H., Olivero, W.C., Sutton, B.P., Georgiadis, J.G., 2013. Local mechanical properties of white matter structures in the human brain. NeuroImage 79, 145–152.

Jones, D.T., Machulda, M.M., Vemuri, P., McDade, E.M., Zeng, G., Senjem, M.L., Gunter, J.L., Przybelski, S.A., Avula, R.T., Knopman, D.S., Boeve, B.F., Petersen, R.C., Jack Jr., C.R., 2011. Age-related changes in the default mode network are more advanced in Alzheimer disease. Neurology 77, 1524–1531.

Jones, D.T., Vemuri, P., Murphy, M.C., Gunter, J.L., Senjem, M.L., Machulda, M.M., Przybelski, S.A., Gregg, B.E., Kantarci, K., Knopman, D.S., Boeve, B.F., Petersen, R.C., Jack Jr., C.R., 2012. Non-stationarity in the "resting brain's" modular architecture. PLoS One 7, e39731.

Liu, Y., Yu, C., Zhang, X., Liu, J., Duan, Y., Alexander-Bloch, A.F., Liu, B., Jiang, T., Bullmore, E., 2013. Impaired Long Distance Functional Connectivity and Weighted Network Architecture in Alzheimer's Disease. Cereb. Cortex 24 (6), 1422–1435.

Manduca, A., Oliphant, T.E., Dresner, M.A., Mahowald, J.L., Kruse, S.A., Amromin, E., Felmlee, J.P., Greenleaf, J.F., Ehman, R.L., 2001. Magnetic resonance elastography: non-invasive mapping of tissue elasticity. Med. Image Anal. 5, 237–254.

Markham, J.A., Greenough, W.T., 2004. Experience-driven brain plasticity: beyond the synapse. Neuron Glia Biol. 1, 351–363.

McKhann, G., Drachman, D., Folstein, M., Katzman, R., Price, D., Stadlan, E.M., 1984. Clinical diagnosis of Alzheimer's disease: report of the NINCDS–ADRDA work group under the auspices of Department of Health and Human Services Task Force on Alzheimer's disease. Neurology 34, 939–944.

McKhann, G.M., Knopman, D.S., Chertkow, H., Hyman, B.T., Jack Jr., C.R., Kawas, C.H., Klunk, W.E., Koroshetz, W.J., Manly, J.J., Mayeux, R., Mohs, R.C., Morris, J.C., Rossor, M.N., Scheltens, P., Carrillo, M.C., Thies, B., Weintraub, S., Phelps, C.H., 2011. The diagnosis of dementia due to Alzheimer's disease: recommendations from the National Institute on Aging-Alzheimer's Association workgroups on diagnostic guidelines for Alzheimer's disease. Alzheimers Dement. 7, 263–269.

Murphy, M.C., Huston III, J., Jack Jr., C.R., Glaser, K.J., Manduca, A., Felmlee, J.P., Ehman, R.L., 2011. Decreased brain stiffness in Alzheimer's disease determined by magnetic resonance elastography. J. Magn. Reson. Imaging 34, 494–498.

Murphy, M.C., Huston III, J., Glaser, K.J., Manduca, A., Felmlee, J.P., Ehman, R.L., 2012a. Phase correction for interslice discontinuities in multislice EPI MR elastography. Proceedings of the 20th Annual Meeting of ISMRM (Melbourne).

Murphy, M.C., Huston III, J., Glaser, K.J., Manduca, A., Meyer, F.B., Lanzino, G., Morris, J.M., Felmlee, J.P., Ehman, R.L., 2012b. Preoperative assessment of meningioma stiffness using magnetic resonance elastography. J. Neurosurg. 118 (3), 643–648.

Murphy, M.C., Huston III, J., Jack Jr., C.R., Glaser, K.J., Senjem, M.L., Chen, J., Manduca, A., Felmlee, J.P., Ehman, R.L., 2013. Measuring the characteristic topography of brain stiffness with magnetic resonance elastography. PLoS One 8, e81668.

Muthupillai, R., Lomas, D.J., Rossman, P.J., Greenleaf, J.F., Manduca, A., Ehman, R.L., 1995. Magnetic resonance elastography by direct visualization of propagating acoustic shear waves. Science 269, 1854–1857.

Putcha, D., Brickhouse, M., O'Keefe, K., Sullivan, C., Rentz, D., Marshall, G., Dickerson, B., Sperling, R., 2011. Hippocampal hyperactivation associated with cortical thinning in Alzheimer's disease signature regions in non-demented elderly adults. J. Neurosci. 31, 17680–17688.

Romano, A.J., Bucaro, J.A., Ehnan, R.L., Shirron, J.J., 2000. Evaluation of a material parameter extraction algorithm using MRI-based displacement measurements. IEEE Trans. Ultrason. Ferroelectr. Freq. Control 47, 1575–1581.

Romano, A., Guo, J., Prokscha, T., Meyer, T., Hirsch, S., Braun, J., Sack, I., Scheel, M., 2014. In vivo waveguide elastography: effects of neurodegeneration in patients with amyotrophic lateral sclerosis. Magn. Reson. Med. 72, 1755–1761.

Sack, I., Beierbach, B., Wuerfel, J., Klatt, D., Hamhaber, U., Papazoglou, S., Martus, P., Braun, J., 2009. The impact of aging and gender on brain viscoelasticity. NeuroImage 46, 652–657.

Song, X.W., Dong, Z.Y., Long, X.Y., Li, S.F., Zuo, X.N., Zhu, C.Z., He, Y., Yan, C.G., Zang, Y.F., 2011. REST: a toolkit for resting-state functional magnetic resonance imaging data processing. PLoS One 6, e25031.

Sperling, R.A., et al., 2011. Toward defining the preclinical stages of Alzheimer's disease: recommendations from the National Institute on Aging-Alzheimer's Association workgroups on diagnostic guidelines for Alzheimer's disease. Alzheimers Dement. 7, 280–292.

Streitberger, K.J., Wiener, E., Hoffmann, J., Freimann, F.B., Klatt, D., Braun, J., Lin, K., McLaughlin, J., Sprung, C., Klingebiel, R., Sack, I., 2011. In vivo viscoelastic properties of the brain in normal pressure hydrocephalus. NMR Biomed. 24, 385–392.

Streitberger, K.J., Sack, I., Krefting, D., Pfuller, C., Braun, J., Paul, F., Wuerfel, J., 2012. Brain viscoelasticity alteration in chronic-progressive multiple sclerosis. PLoS One 7, e29888.

Tzourio-Mazoyer, N., Landeau, B., Papathanassiou, D., Crivello, F., Etard, O., Delcroix, N., Mazoyer, B., Joliot, M., 2002. Automated anatomical labeling of activations in SPM using a macroscopic anatomical parcellation of the MNI MRI single-subject brain. NeuroImage 15, 273–289.

Weissenbacher, A., Kasess, C., Gerstl, F., Lanzenberger, R., Moser, E., Windischberger, C., 2009. Correlations and anticorrelations in resting-state functional connectivity MRI: a quantitative comparison of preprocessing strategies. NeuroImage 47, 1408–1416.

Wuerfel, J., Paul, F., Beierbach, B., Hamhaber, U., Klatt, D., Papazoglou, S., Zipp, F., Martus, P., Braun, J., Sack, I., 2010. MR-elastography reveals degradation of tissue integrity in multiple sclerosis. NeuroImage 49, 2520–2525.

Xu, L., Lin, Y., Han, J.C., Xi, J.N., Shen, H., Gao, P.Y., 2007. Magnetic resonance elastography of brain tumors: preliminary results. Acta Radiol. 48, 327–330.

Yin, M., Talwalkar, J.A., Glaser, K.J., Manduca, A., Grimm, R.C., Rossman, P.J., Fidler, J.L., Ehman, R.L., 2007. Assessment of hepatic fibrosis with magnetic resonance elastography. Clin. Gastroenterol. Hepatol. 5, 1207–1213.